Proceedings of the ASME 2019 38th International Conference on Ocean, Offshore and Arctic Engineering
OMAE2019
June 9-14, 2019, Glasgow, Scotland

DRAFT OMAE2019-95100

REAL TIME CEMENTING HYDRAULICS SIMULATIONS BRING RISK DOWN

Sviatoslav Pelipenko
Oxford Numerics Ltd
London, UK

Nicolas C. Flamant
Schlumberger
Sugarland, Texas, USA

Simon C. Impey
Oxford Numerics Ltd
London, UK

ABSTRACT

Proper control of downhole pressure during cementing operations is critical to maintaining well integrity, i.e. avoiding getting a well kick or fracturing the formation. Contrary to drilling operations where pressure can be monitored in real time thanks to measurement while drilling by downhole tools, no such measurements are available while cementing. Cementing operations must therefore rely on the use of simulations to estimate pressures downhole and ensure that the well integrity is not compromised. These simulations are typically performed ahead of the operations, but for critical wells it is paramount to also perform the calculations in real time to account for any deviation from the plan.

We will first provide a description of the hydraulics simulator used for real time simulations. A key feature is the ability to account for fluctuations in injected fluid density, as a result of the cement slurry mixing process. This effectively results in tracking a high number of fluids with different density properties. The simulator also takes into account fluid compressibility and pressure and temperature dependent fluid viscosity, the magnitude of the effects of which we examine in application to generic field cases. Another salient feature of the simulator is its ability to determine whether fluid is lost to the formation by using flow returning from the well as an additional input.

We highlight the work accomplished to achieve the performance required for real time computations and then illustrate how the simulator gets used during operation through a case study.

INTRODUCTION

Primary well cementing is a critical part of oil and gas well construction whereby cement is placed in the annular gap between the steel casing and formation or the casing of the previously drilled stage. The main goal is to provide zonal isolation to prevent the migration of the gasses and liquids present in formation between different zones or to the surface. If not prevented, such migration causes a reduction in reservoir pressure and the subsequent loss of well productivity or in the case of flow to surface an uncontrolled blowout with significant environmental damage.

Ability to simulate the cementing process is important at the well design stage when the fluid properties, stage depths, casing dimensions and centralization can be adjusted to ensure the planned job will hit the targets safely. More recently, real-life monitoring and simulation of the job as it is happening using data acquired in real time is considered of the increased importance. Detecting discrepancies between the simulated and observed parameters during the job allows for an early identification of issues such as losses to formation with appropriate remedial action taking place during or soon after the job.

From the physics standpoint, the problem of well cementing can be characterized as a displacement fluid flow of a sequence of compressible, non-Newtonian fluids. The geometry of the flow path is a sequence of inclined pipe and annular sections, which are narrow and long. The flow is typically laminar but can also be turbulent for some of the fluids in the flow path or during certain parts of the process such as mud circulation through drill pipe prior to cement placement. The pressure and temperature variation in the flow path can be significant with over 100 °C and 100 MPa differentials between inlet and bottom hole conditions not uncommon. Additional complexity is provided by the optional inclusion of a check valve activating on back flow, fluid losses from the flow path to formation over a range of depths, foamed fluid placement and a variety of on- and offshore cementing job configurations. Finally, in the context of real-time

simulation, the measured density of the fluid injected into the flow path varies with time at a measurement frequency of typically 1 Hz.

Full 3-D computational simulations of a complex flow problem such as this on the scale of real-life cases is prohibitively costly in terms of simulation times. As such, current strategies focus on smaller-scale experimental flow paths with a coarse mesh (e.g. [3]), single-fluid flows or make simplifying assumptions such as the narrow gap approximation for the annulus and fluid incompressibility as in [4-7].

The approach taken with the real time hydraulic simulator is to reduce the problem to a one-dimensional one. This significant simplification allows us to retain detail elsewhere, simulating the effects of compressibility, fluid viscosity variable with pressure and temperature, full generality of flow paths and features such as losses and valves. Importantly, it enables a simulation of cementing flow on the scale of real-life wells with thousands of fluids of varying densities to run in a few seconds to minutes on an average modern computer. This allows for simulation of the flow with acquired data as input in real time using consumer-level hardware by engineers on site or onshore experts.

MODEL

The key assumption made is that the interfaces between fluids are level as they transit the flow path – there are no dispersion, diffusion or mixing effects. As such, the model is reduced to a single axial dimension. The 1D compressible Navier-Stokes momentum conservation equation is:

$$\rho u_t + \rho u u_x = -p_x + S_u \tag{1}$$

where ρ is the density, u is the flow velocity, p is the pressure, x is the axial coordinate, t is the time and the subscript notation is used for partial derivatives with respect to x and t. The momentum source, S_u, contains the wall friction forces and gravity body forces:

$$S_u = -\frac{2f\rho|u|u}{D} + \rho g' \tag{2}$$

where f is the Fanning friction factor, D is the hydraulic diameter and g' is the component of gravity acting in the axial direction. The mass conservation equation accounting for variable flow-path cross-section is:

$$A\rho_t + (A\rho u)_x = S_m \tag{3}$$

where A is the cross-section area which varies along the flow path and the mass source S_m, allows for transfer of fluid with the formation (e.g. due to losses). Substituting for ρ_t from (3) into (1) we have:

$$-p_x + S_u = (\rho u)_t + \frac{1}{A}(A\rho u^2)_x - \frac{S_m u}{A} \tag{4}$$

We now discard the acceleration term $(\rho u)_t$ thus ignoring the dynamic flow effects such as shock waves and pressure oscillations on rapid flow rate changes. The effect of the terms on computed pressure can be non-negligible during rapid velocity changes. This is left to be resolved by a separate simulator due to significantly finer simulation time and spatial scale required and the additional input characterizing the well equipment behaviour that may not be readily available.

The last term in Eq. (4) is the momentum change due to losses – the momentum transferred with the fluid going into the formation. An order of magnitude check with the typical values of u = 1 m/s, ρ = 2000 kg/m^3 shows that for total losses with the entire flow going into the formation, the inertial pressure loss is $\rho u^2/2$ = 1 kPa, a modest pressure change on the scale of the well and so the term is currently ignored.

The governing equations are therefore the mass conservation Eq. (3) together with the momentum equation

$$-p_x + S_u = \frac{1}{A}(A\rho u^2)_x \tag{5}$$

The fluids are characterized with Hershel-Bulkley rheology model:

$$\tau = \tau_y + \kappa\dot{\gamma}^n \tag{6}$$

where τ is the shear stress, $\dot{\gamma}$ is the rate of strain, τ_y is the yield stress, κ is the consistency and n is the power index. The viscosity can be specified as a set of constant rheological parameters (τ_y, κ, n), or as a set of Fann rheometer reading measurements at different pressures and temperatures. Similarly, for density, the simulator supports a variety of models – constant, compositional or a pressure-temperature interpolation.

To compute the friction factor f for a given fluid viscosity, flow path geometry and flow rate, the Metzner and Reed [8] Reynolds approach for Power Law fluids is used. For pipe flow, an equivalent generalized Reynolds number for Hershel-Bulkley fluids is derived as follows:

$$N_{Re.pipe} = \frac{\rho u^{2-n'} D^{n'}}{8^{n'-1} k'} \tag{7}$$

where n' and k' are local power-law parameters defined by

$$n' = \frac{d(\log(\tau_w))}{d\left(\log\left(\frac{8u_{lam}}{D}\right)\right)} \tag{8}$$

$$k' = \frac{\tau_w}{\left(\frac{8u_{lam}}{D}\right)^{n'}} \tag{9}$$

where τ_w is the wall shear stress and u_{lam} is the corresponding average velocity for a laminar flow regime. For laminar flow in pipe, the friction factor is then

$$f = \frac{16}{N_{Re.pipe}} \tag{10}$$

and for the turbulent regime

$$f = a{N_{Re.pipe}}^{b} \tag{11}$$

where a and b are empirical functions of n', following [9] with log-log interpolation used for transitional flow. For transition thresholds for laminar/transitional and transitional/turbulent flow regimes, established expressions in terms of generalized critical Reynolds numbers are used, see [10]. For annular pressure drop the same approach is used with the assumption of a concentric narrow gap annulus.

It is worth noting that the overall hydraulic simulator model and implementation is flexible to the type of friction pressure gradient calculations used and alternative models can be easily substituted. The only requirement of the solution algorithm is continuity and monotonicity of computed friction pressure gradient with velocity.

For the coupled temperature simulation, a bulk element temperature model with empirically-calibrated heat transfer coefficients is used, starting with the radial advection-diffusion equation

$$T_t + \boldsymbol{v}\boldsymbol{\nabla}T = \alpha\nabla^2 T \tag{12}$$

where T is the temperature, $\boldsymbol{v}$ is the velocity vector and α is the diffusivity. Assuming a single axial velocity in pipe and annulus and ignoring the axial diffusion, equations are derived for each of the regions (pipe, annulus and formation) in terms of the average temperature and inner and outer boundary temperatures. The result is a system of linear first order partial differential equations for each depth with the unknowns being the average temperatures in pipe, annulus and near-field formation with each equation of the form

$$T_t + uT_x = \frac{2\alpha}{r_{ext}^2 - r_{int}^2}\left(r_{ext}T_r|_{r_{ext}} - r_{int}T_r|_{r_{int}}\right) \tag{13}$$

where r_{int} and r_{ext} are the internal and external radii of the corresponding regions – so for the annulus region in a single casing in an open hole geometry r_{int} is the outer radius of the casing and r_{ext} is the open hole radius. For more details of the bulk temperature model used please see [11].

NUMERICAL DISCRETIZATION AND SOLUTION

The numerical discretization and solution adopted can be categorized as a mixture of the Eulerian and Lagrangian approaches. The 1-D flow path is discretized into cells each with a constant geometry through which the fluids are advected. Fluids in the flow path are represented by a sequence of contiguous fluid blocks. Each fluid block is a length of fluid with a single viscosity, density and thermal parameter models – typically corresponding to a single pumping stage. Fluid properties of a particular fluid block in a single flow path cell are considered to be constant during a time step.

The initial conditions are known fluid positions, velocities and temperatures in pipe, annulus and formation. The starting fluid positions may also include a free surface in pipe and annulus. The boundary conditions can vary during the simulation but are in general as follows:

- Set pressure at outlet – typically annular backpressure;
- Imposed flow rate at inlet – pumping rate at cement head;
- Set pressure at free surface – if a u-tube is encountered in annulus or pipe due to losses or hydrostatic imbalance;
- No flow across the valve if a valve is shut;
- Fixed flow rate at a loss zone if one is defined. Alternatively, for a special loss type, a set flow rate at outlet.

Additional conditions may be imposed by various well equipment items or be specific to particular job configurations. For example, for a managed pressure cementing configuration such as described in [12], a variable choke pressure is introduced at the top of the annulus on the drill floor.

The solution method is a time-implicit mass tracking iterative sweep. The exact method varies depending on the boundary conditions, but in general for each time step, pressure and flow rate is set at one end of the flow path, typically at the outlet. For a standard set of boundary conditions – flow rate at inlet, pressure at outlet – the set pressure comes from the input and the outlet flow rate is initially guessed from the previous time step or the inlet flow rate. Discretized mass and momentum Eq. (3) and (5) above are used to compute pressure, flow rate and fluid mass in each cell working backwards through the flow path. The total mass of fluid in each fluid block is tracked and interfaces are placed accordingly. When the calculation sweep reaches the beginning of the flow path, a closed valve or a free surface, the total mass of the fluid blocks in the flow path is summed up. With the mass of the fluids at the previous time step and injected fluid mass known, mass conservation for the entire flow path is then used to adjust the boundary conditions at the outlet. The sweep is repeated until the flow path mass conservation is satisfied to within a set tolerance.

The temperature simulation is decoupled from the placement simulation with time, depending on the setting chosen. Either the previous time step's fluid positions and velocities are used to compute the evolution of the temperature prior to the placement simulation or it is done after the placement simulation. The temperature simulation can also be run in parallel with the placement whereby the previous time step's velocities are used in the temperature simulation with the results of the simulation fed into the next time step of the placement simulation, further enhancing the computational performance. An examination of the simulation results with realistic input revealed negligible differences in computed parameters for the different decoupling methods.

IMPLEMENTATION

The main challenges in the implementation of the numerical method in the simulator are the performance and robustness for the full generality of input. This is especially acute for playback cases where the continuous variation in injected fluid density requires thousands of blocks of compressible fluids with differing properties to be advected through the flow path. The viscosity and density of each fluid block varies with time and it transits potentially hundreds of different geometries as the dimensions of the well can vary significantly in the open hole sections.

For the complex, compressible playback cases, the majority of the computational time is spent on calculating fluid viscosity with varying pressure and temperature and friction pressure gradient from viscosity for a given flow rate and well geometry. To significantly improve the computational performance in such cases, an innovative interpolation method is used. For each geometry in the flow path and each fluid, a multi-dimensional tree structure with computed friction pressure values versus pressure, temperature and velocity is gradually constructed during the simulation. A hash key is generated for each geometry and fluid so that an appropriate interpolation tree can be retrieved during the simulation. When a friction pressure calculation is requested for a certain pressure, temperature and flow rate point, a tree traversal algorithm locates the already-computed values in a cube around the target point. If the differences in friction pressure values exceed the interpolation threshold, the cube is iteratively subdivided, and the viscosity and friction pressure is computed in each corner until the differences in computed friction pressure at corner points fall below the interpolation threshold. During the subdivision, the time-intensive calculations of viscosity with pressure and temperature and friction pressure are done in parallel to utilize the multi-core capabilities of modern computers. Finally, interpolation between the corners of the bounding cube is used to compute friction pressure and auxiliary parameters such as effective viscosity.

The advantage of using this dynamically generated tree interpolation method is that the pressure, temperature and velocity domain is divided only when required, providing an optimal resolution in the directions where the viscosity or friction pressure varies more rapidly. For fluids where the viscosity has been measured in lab conditions at a range of pressures and temperatures, this typically results in greater resolution in temperature and velocity and a coarser resolution in pressure directions. The impact of using the interpolation tree can be dramatic – over an order of magnitude overall simulation performance improvement when compared with not using friction pressure or viscosity interpolation.

A range of other performance-oriented features have been implemented to enable real-time playback computation.

When constructing the flow path mesh, the friction pressure response is abstracted from the flow path volume for sections where the geometry varies rapidly, such as the open hole with dense caliper readings. This enables amalgamation of neighboring flow path cells whilst preserving the overall friction pressure response. This avoids smaller cells resulting in increased computation times due to the need for a reduced time step due to the Courant–Friedrichs–Lewy condition of the time advance scheme. Additionally, the effect of the tubular joints on both flow path volume and friction pressure response can be captured without significantly increasing the number of computational cells.

When processing the input for playback schedule either in real-time update or playback modes, the acquired density and flow rate channels are filtered and adjoint stages of nearly-identical densities are amalgamated. A range of lower-level optimizations include the use of parallelization such as in the case of the temperature, friction pressure, viscosity and static pressure calculations and the use performance-oriented Intel© C++ compilers.

The combination of algorithm improvements and targeted optimizations has resulted in a robust hydraulic simulator that can execute a hydraulic and temperature simulation of full-scale cementing job for compressible fluids with pressure and temperature dependent viscosity in a few seconds for a design pumping schedule and typically under a minute for a complete playback job with acquired data at 1Hz. The acquired data can also be fed into the simulator at any rate in irregular intervals – with the simulator performance ensuring negligible processing backlog.

Lastly, the same simulator can be used on a full range of cementing jobs including foam placement, various managed pressure cementing configurations and simulation of experimental-scale flow loops.

CASE STUDY

The simulator is systematically run ahead of cementing operations to ensure that pressure within the well remains within the window defined by the formations pore and fracture pressures. The density and viscosity of the cementing fluids, as well as the pump rates, are the main parameters that are fine-tuned at this stage. Multiple scenarios must be explored, and the fast simulation run times are key for finalizing the job design efficiently.

Yet the simulator performance really becomes critical when playing back an actual operation after the fact or performing the simulation in real time. In such cases, the flow rates and fluid density inputs are measured parameters, typically acquired at 1 Hz. If available, the acquired injection temperature can also be fed to the simulator. In cases where losses to the formation are experienced, the well return flow rate is used by the simulator as an outlet boundary condition, and the loss rate to the formation is then calculated by satisfying the mass balance in the flow path. Finally, the acquired surface pressure is a matching parameter for the simulated surface pressure.

Real-time simulations allow the outcome of the cementing operation to be evaluated continuously throughout the operation. A situation where real-time diagnostic is most needed is the occurrence of losses during cementing operations. Depending on the location and amount of losses, a remedial operation may or

may not be required. Early diagnostic allows early planning, therefore saving rig time.

Such a situation was encountered while cementing a liner in a deep offshore environment. The well schematic is presented in Fig. 1. Partial losses had been experienced while drilling the section to be cemented, and losses were therefore also expected while cementing. The loss zone was suspected to be located just above the planned top of cement. The analysis presented here was performed just after the operation, in playback mode, but could have been performed similarly in real time.

The 1 Hz acquisition data was averaged over time periods of 10 seconds. The simulation mesh adapted to the well geometry, with a maximum cell length of 25 m and minimum of 10 m. The calculation time step was constrained by the Courant–Friedrichs–Lewy condition and the 10 s output sampling rate. The maximum computation time step value was 10 s and minimum 1 s. The simulation run time when simulating losses on a 1-year old quad-cores laptop computer was around 90 seconds, to be compared with a pump time of 6 hours and 52 minutes.

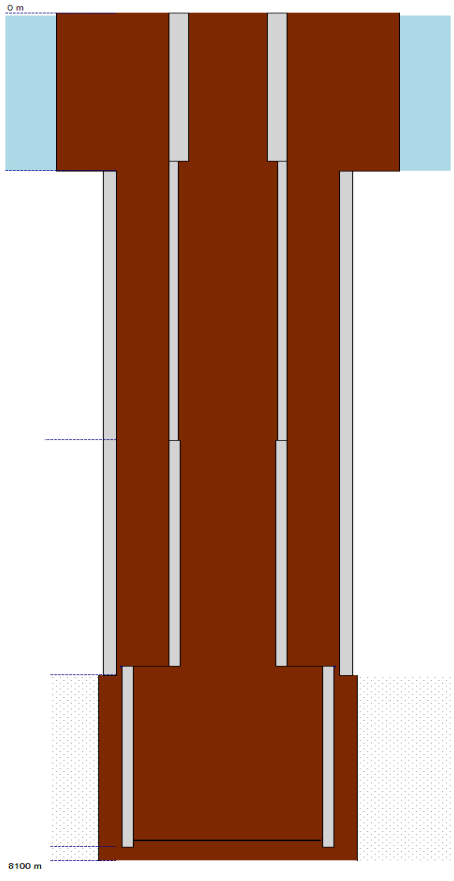

FIGURE 1. Well schematic depicting the flow path during the cementing operation. Total depth is 8100 m, a riser goes from sea bed to surface, the liner is connected back to surface with a drill pipe.

The fluids return rate was estimated by the simulator based on the dynamic measurement of the mud volume in the mud pits. While fluids other than mud are pumped into the well, the return rate is directly equal to the time derivative of the mud volume. While mud is pumped into the well from the pits, the return rate is equal to the sum of the mud pump rate and the derivative of the mud volume. The latter is negative if the return rate is less than the pump rate.

Figure 2 presents the acquired pump rate (top panel), return rate (second panel from top), surface pressure (third panel from top), and injected density (bottom panel) vs. the time elapsed since the beginning of the operation in hh:mm. The four sets of data were recorded by the cement equipment and rig sensors. The pump rate and density are inputs to the simulator while the pressure and mud pits volume are matching parameters. The operation consisted of injecting a 12 m^3 spacer stage (from 0:00 to 00:52), followed by a 25.8 m^3 cement slurry stage (from 1:16 to 02:01), and finally a second 4 m^3 spacer stage (from 2:03 to 2:07). All three stages were then displaced with 184 m^3 of drilling mud, until end of acquisition. The pressure plateau starting at 00:14 corresponds to the pressure test of the surface lines. Note that the pressure data during the test was truncated at 10,340 kPa to allow for a better visualization. Several pressure spikes are noticed on the surface pressure signal. They are related to darts and wiper plugs. A first dart was dropped between the first spacer stage and the slurry lead interface, and a second dart between the slurry tail interface and the second spacer stage. When reaching the liner hanger, the first dart latched to the bottom wiper plug and the second dart to the top wiper plug. Both latching events are clearly identified as surface pressure triple spikes, the first set ending at 03:26 and the second set at 04:01. The next pressure spike at 05:57 corresponds to the bottom plug reaching the landing collar, while the final pressure spike at 06:52 corresponds to the landing of the top plug and the end of the cementing operation. The mud pit volume data clearly highlights the occurrence of losses. A first phase, ranging from the start of the operation to 2:10, during which the mud volume in the pits increases, corresponds to the injection of the spacers and slurry. The balance is positive as mud is returned to the pits while no mud is pumped into the well. Yet the average slope for that phase is around 280 L/min, which is less than the average pump rate of 600 L/min. An average loss rate of 320 L/min was therefore experienced. A second phase during which the volume of mud in the pits decreases until the end of the operation corresponds to the displacement stage. In the absence of losses, the volume should have remained mostly constant. The average slope corresponds to the difference between the pump rate and the loss rate, and amounts to average losses of 440 L/min.

The darts and plug landing events allowed for the calibration of the displacement volume, which initially was 3 m^3 off, despite the simulator accounting for the change in drilling mud density with pressure and temperature. In deed many uncertainties remain, such as the drill pipe and liner actual inner diameters (as opposed to nominal), the pump rate, and of course the accuracy

of the density compositional model. The density compositional model follows the approach laid out in [13]. A three-phases mixture of base-oil, brine and solids is considered. Fitted density models have been established for each phase, allowing the calculation of the density of the mixture. In Fig. 3 we display the output of the model as isovalue density lines with a 10 kg/m^3 step. The pressure and temperature ranges match that experienced by the drilling mud during the operation. At surface, at 20 °C and atmospheric pressure, density was 1820 kg/m^3, while at bottom hole, at 80 °C and 1488·10^5 Pa, density was 1880 kg/m^3. Note that we consider the spacer and cement slurries as incompressible: being water-based their density is much less sensitive to pressure and temperature than oil-based drilling fluids.

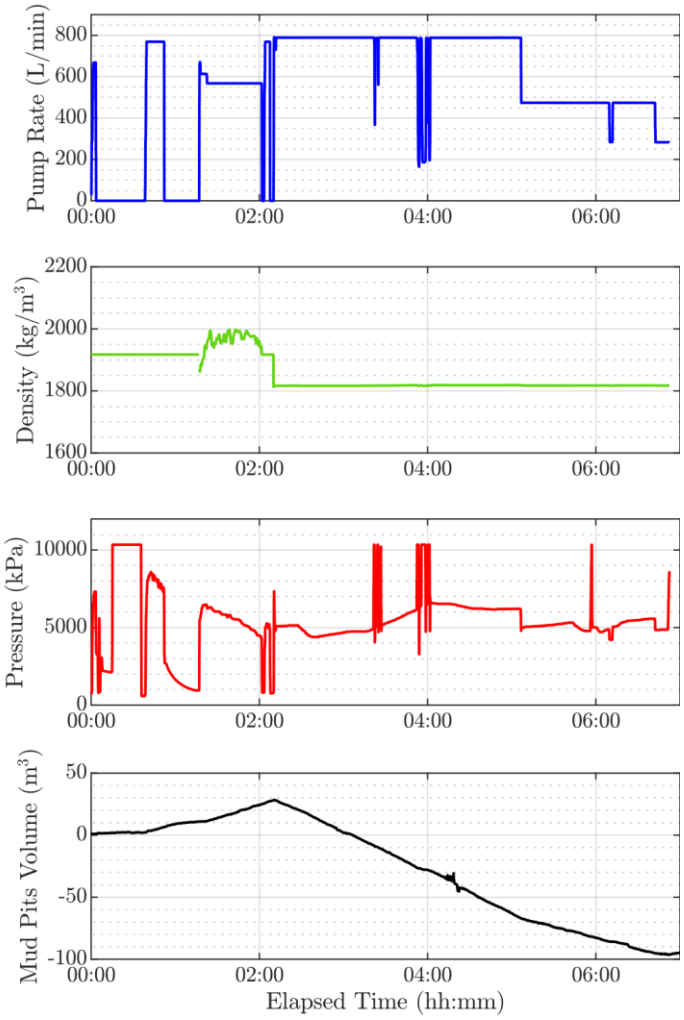

FIGURE 2. Acquisition data from the operation. Spacer was pumped from 0:00 to 00:52, cement slurry from 1:16 to 02:01, spacer again from 2:03 to 2:07, and finally drilling mud until the end of the operation. Upper panel, in blue: acquired pump rate (L/min). Second panel from top, in green: acquired surface density for the cement slurry from a Coriolis flow meter, merged with constant design density for spacer and drilling mud. Third panel from top, in red, surface pressure, typically measured near the outlet of the pump. Bottom panel, in black: acquired mud pits volume (m^3), derived from ultrasonic level sensors setup for all the pits.

Interestingly, running the same simulation without accounting for fluid compressibility would have resulted in an over displacement of 5.6 m^3, a larger error than that experienced with compressibility.

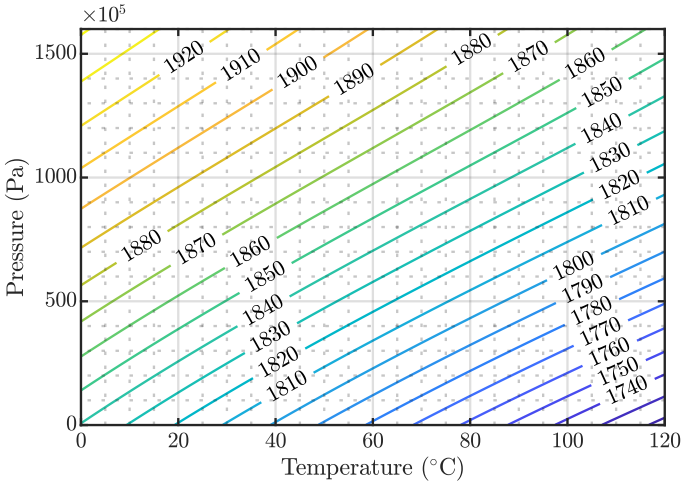

FIGURE 3. Drilling mud density vs. temperature (°C) and pressure (10^5 Pa). Isolines are drawn every 10 °C. As expected intuitively the density increases as pressure increases and decreases as temperature increases.

Drilling mud viscosity also presented strong differences between surface and downhole conditions. The viscosity model [14] relies on an empirical multi-dimensional regression built over a large set of experimental data acquired over the years using high pressure, high temperature Couette rheometers. The model was calibrated with measurements performed on the day of the operation. Three sets of data were acquired using a standard oilfield Couette rheometer at atmospheric pressure and temperature of 38 °C, 66 °C and 4 °C respectively. According to the simulation data, the shear rate in the flow path ranged from 20 to 50 s^{-1} in the annulus and 50 to 120 s^{-1} in the pipe. To provide a sense of the viscosity changes within the flow path due to pressure and temperature, viscosity calculated at a constant shear rate of 50 s^{-1} is presented in Fig. 4. Viscosity isolines are plotted vs. the pressure and temperature intervals experienced by the drilling mud during the operation. Note that the viscosity step between each isoline is not constant, due to the steep viscosity gradient at low temperatures and high pressures. At our imposed shear rate, surface viscosity was 192 mPa·s, and drilling mud viscosity was highest in the annulus at the sea bed depth reaching 280 mPa·s for a temperature of 4 °C and a pressure of 279·10^5 Pa. Finally, maximum bottom hole viscosity was 240 mPa·s at 70 °C and 1485·10^5 Pa and minimum bottom hole

viscosity was 200 mPa·s at 103 °C and 1445·10^5 Pa. We notice that temperature and pressure have opposite effects and tend to compensate each other initially when temperature at bottom hole is high. But once cooler fluids reach bottom hole, viscosity increases.

The spacer and cement slurries were modeled with constant rheological properties, measured at 81 °C. For the spacer, consistency was 590 mPa·s$^{0.64}$, power index 0.64 and yield stress 2 Pa. For the cement slurry, consistency was 620 mPa·s$^{0.79}$, and power index 0.79. The Metzner and Reed Reynolds number did not exceed 1000 throughout the simulation, except in the annular restriction created by the liner hanger, hence over a very short length. The flow regime was laminar throughout the flow path, except in the restriction where it was turbulent.

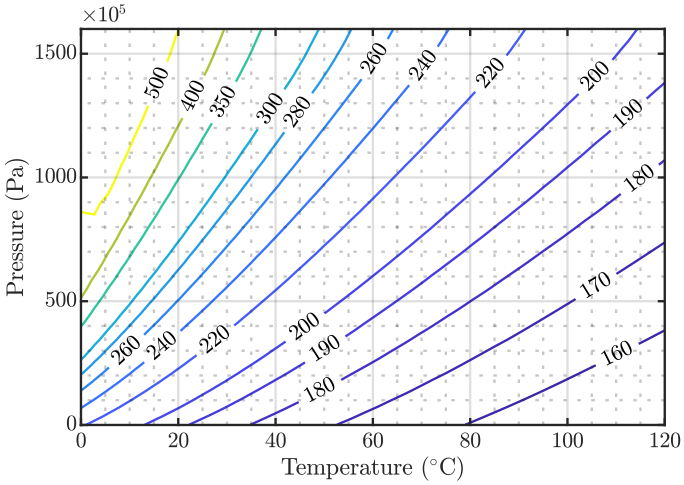

FIGURE 4. Drilling mud effective viscosity (mPa·s) at a shear rate of 50 s^{-1} vs. temperature (°C) and pressure (10^5 Pa). Isolines are drawn at values of 160, 170, 180, 190, 200, 220, 240, 260, 280, 300, 350, 400, and 500 mPa·s.

The first step in our analysis of the cementing operation is to come up with the loss rate, by matching the simulated and acquired mud pits volumes over time. We present the result of the match in Fig. 5. The match, although not perfect, is good enough for carrying on our analysis. Yet the determination of the return rate from the mud balance definitely requires further work, in particular about how to better deal with the time lag between a change in return rate and the associated response of the mud pits volume data. This lag is associated with some accumulation occurring in the surface equipment.

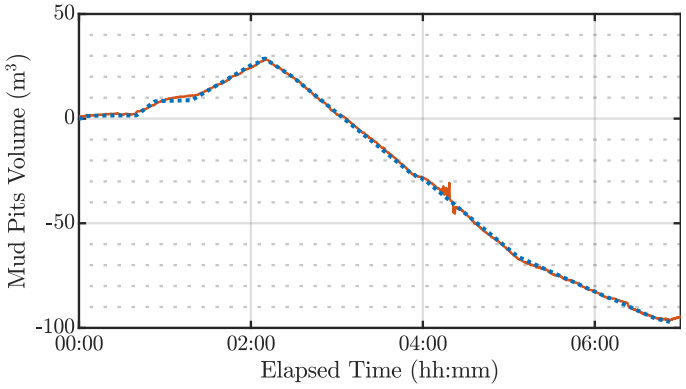

FIGURE 5. Comparison of simulated vs. acquired mud pit volume: (–) acquired volume; (···) simulated volume.

In Fig. 6 we now present the two flow rates obtained by performing the match: the return flow rate, in the top panel, corresponding to drilling fluid exiting the well at surface, and the down hole loss rate, in the bottom panel. Not unsurprisingly, the amount of losses was at the highest while the pump rate was maximum, from 02:10 to 05:05. In relative terms the loss rate was around 68% of the pump rate. In contrast, at the end of the execution, when pump rate was lowered to around 475 L/min, the loss rate decreased to 55% of the loss rate. Losses could therefore have been reduced significantly by displacing at lower pump rates.

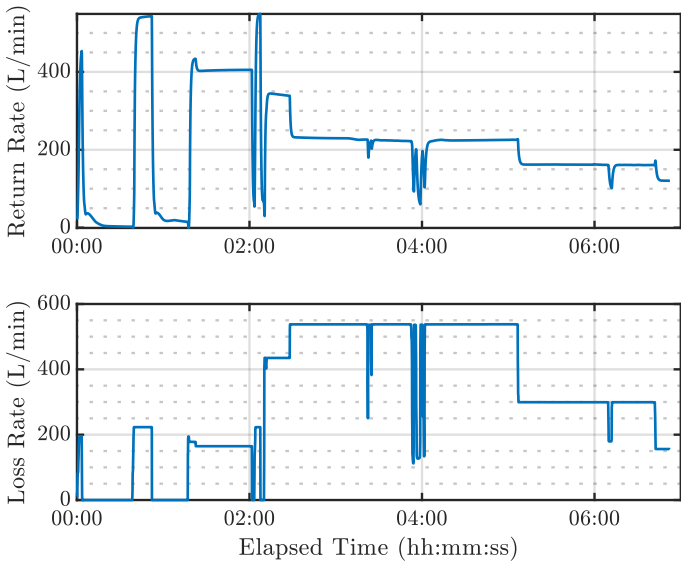

FIGURE 6. Top panel: simulated return rate (L/min). Bottom panel: simulated loss rate (L/min).

The key for this operation was the identification of the loss zone location. To this end three scenarios were investigated, with

loss zone at the liner shoe, in the middle of the planned cemented interval and above the planned top of cement. The fourth scenario corresponds to the absence of losses.

The associated pressure matches are presented in Fig. 7. In all panels, the acquired surface pressure is plotted as a continuous line and the simulated surface pressure as a dotted line. The top panel provides the comparison without simulating any losses. The second panel from the top displays the results for a loss zone located at the liner shoe. The third panel from the top considers a loss zone in the middle of the cemented interval and the bottom panel a loss zone above the planned top of cement. The changes in surface pressure are mainly related to the friction pressure losses at the liner hanger and in the liner / open hole annulus. The large difference observed between the scenarios with losses and the scenario without losses is related to the change in flow rate through the liner hanger. The effect of the loss zone location is subtler: the deeper the loss zone, the lower the flow rate in the annular space above it, and hence the lower friction losses and consequently surface pressure. The best match corresponds to the loss zone being located at the liner shoe, and that is especially true at the end of the operation. A shallower loss zone will result in a rise of simulated pressure, and so would more distributed losses. The simulation results are consistent with the worst-case scenario of the loss zone located at the liner shoe. The conclusion of the comparison between acquired data and simulated data is therefore that partial losses took place at the liner shoe, resulting in a cement height of 220 m. These results proved consistent with a cement bond log that was run later on, and the operation was considered successful.

CONCLUSION

Playback or real time cement placement simulations can bring useful insight into the outcome of cementing operations, especially for complex situations such as the partial losses case presented here. The relevance of the analysis relies on a new set of simulation features, such as the handling of losses and the modeling of density and viscosity that change with pressure and temperature. The simulator fast run times is a key enabler, which allows the running of multiple scenarios efficiently, including in real time. In the case study presented here, the operation was assessed after the fact. A real time simulation would have provided the opportunity to make changes to the execution of the operation. In particular it would have made sense to lower the pump rate even more once the cement slurry reached the annulus. Without real time simulation data, decisions such as these are more difficult to take: the benefits of decreasing the pump rate cannot be estimated and counterbalance the risk of increasing the displacement time. In the absence of downhole real time measurements while executing cementing operations, real time simulations are the only means of interpretation. Although simulations will always be imperfect, the performance and accuracy of modern simulators have reached the point where they enable better control of the operations, as evidenced by the consistent interpretation obtained via simulation the cement bond log. Yet their adoption remains low due to the slow pace at which confidence builds.

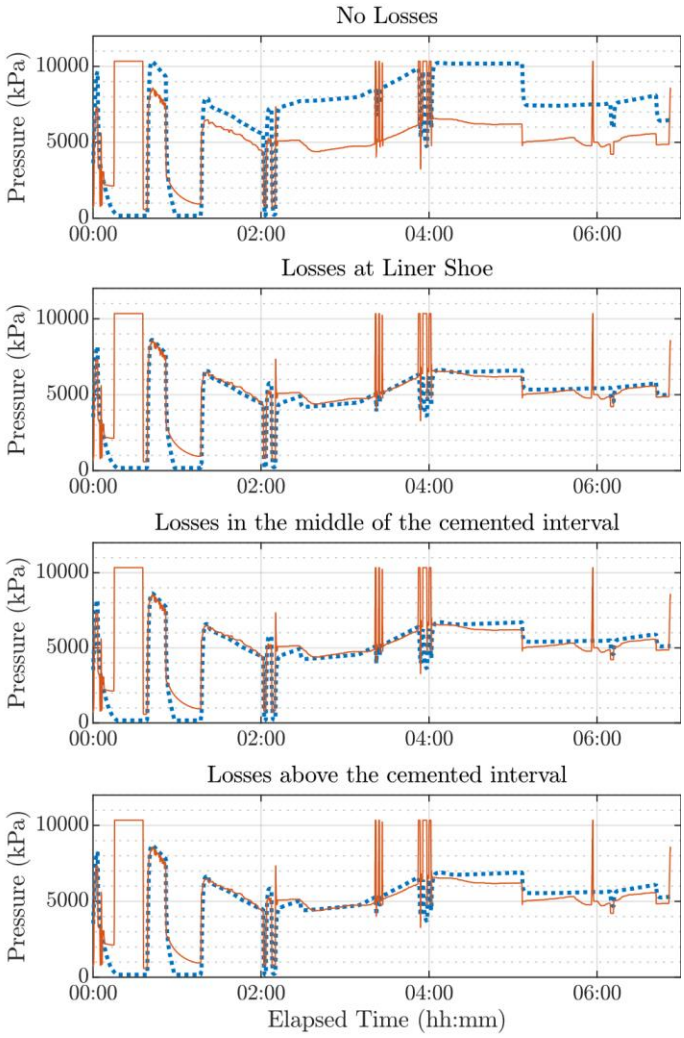

FIGURE 7. Presentation of the different loss scenarios. Top panel: no losses. Second panel from top: losses occurring at liner shoe. Third panel from the top: losses occurring in the middle of the planned cemented interval. Bottom panel: losses occurring above the planned top of cement. On all panels we compare acquired pressure, red line(–), vs. simulated pressure, blue dots (⋯).

ACKNOWLEDGEMENTS

The authors thank the Schlumberger cementing engineers involved with the operation discussed in the case study, whose insight was invaluable.

NOMENCLATURE

A	cross-section area of the flow path at a point (m^2)
D	hydraulic diameter (m)
f	Fanning friction factor (dimensionless)

g'	acceleration due to gravity in the axial direction (m/s^2)
n	power index of the fluid (dimensionless)
p, p_x	pressure (Pa), partial derivative of pressure with respect to the axial coordinate
T, T_t, T_x, T_r	temperature (K), partial derivative of temperature with respect to time, axial coordinate, radius
u, u_t, u_x	flow velocity (m/s), partial derivative of flow velocity with respect to time and axial coordinate
$\boldsymbol{v}$	fluid velocity vector (m/s)
x	axial coordinate (m)
α	thermal diffusivity (m^2/s)
$\dot{\gamma}$	rate of strain (s^{-1})
μ	fluid viscosity (Pa·s)
κ	consistency of the fluid ($Pa \cdot s^n$)
τ	shear stress (Pa)
τ_w	wall shear stress (Pa)
τ_y	yield stress of the fluid (Pa)
ρ	fluid density (kg/m^3)

REFERENCES

[1] Contreras, J., Bogaerts, M., Griffin, D., Rodriguez, F., Sianipar, S., Villar, V., and Taoutaou, S, 2017. "Real-Time Monitoring and Diagnoses on Deepwater Cement Barrier Placement: Case Studies from the Gulf of Mexico and Atlantic Canada." In Offshore Technology Conference, Houston, Texas, May 1–4, 2017. OTC-27797-MS.

[2] US Bureau of Safety and Environmental Enforcement. United States Code. 30 Cfr 250 - Oil And Gas And Sulphur Operations In The Outer Continental Shelf. July 1, 2016.

[3] Savery, M, Chin, W. and Yerubandi, K. B., 2008. "Modeling cement placement using a new 3-D flow simulator." In AADE Fluids Conference and Exhibition, Houston, Texas, April 8–9, 2008. AADE-08-DF-HO-08.

[4] Bittleston, S. H., Ferguson, J., and Frigaard, I. A., 2002. "Mud removal and cement placement during primary cementing of an oil well – Laminar non-Newtonian displacements in an eccentric annular Hele-Shaw cell". *J. Eng. Math.* ***43***(2)**,** pp. 229–253.

[5] Pelipenko, S. and Frigaard, I. A., 2004. "Two-dimensional computational simulation of eccentric annular cementing displacements." *IMA J. Appl. Math* ***69***(6), pp. 557–583.

[6] Maleki, A., Frigaard, I. A., 2018. "Turbulent displacement flows in primary cementing of oil and gas wells." *Physics of Fluids* ***30***(12), p. 123101.

[7] Tardy, P. M. J. and Bittleston, S. H., 2015. "A model for annular displacements of wellbore completion fluids involving casing movement." *Journal of Petroleum Science and Engineering* ***126***, pp. 105–123.

[8] Metzner, A. B. and Reed J. C., 1955. "Flow of non-Newtonian fluids—correlation of the laminar, transition, and turbulent-flow regions." *AIChE J.* ***1***(4), pp. 434–440.

[9] Dodge, D. W. and Metzner, A. B., 1959. "Turbulent flow of non-Newtonian systems." *AIChE J.* ***5***(2), pp. 189–204.

[10] Nelson, E. B. and Guillot, D. 2006. *Well Cementing Second Edition*. Schlumberger, Sugar Land, Texas US.

[11] Romero, J. and Touboul, E., 1998. "Temperature prediction for deepwater well: a field validated methodology." In SPE Annual Technical Conference and Exhibition, New Orleans, Louisiana, September 27–30, 1998. SPE-49056-MS.

[12] Kaasa, G-O., Stamnes, O., Imsland, L. and Aamo, O. M., 2011. "Intelligent Estimation of Downhole Pressure Using a Simple Hydraulic Model." In IADC/SPE Managed Pressure Drilling and Underbalanced Conference and Exhibition, Denver, Colorado, April 5–6, 2011. SPE-143097-MS.

[13] Zamora, M., Roy, S. and Slater, K., 2013 "Issues with the density and rheology of drilling fluids exposed to extreme temperatures and pressures." In ASME 2013 32nd International Conference on Ocean, Offshore and Arctic Engineering, Nantes, France, June 9–14, 2013. OMAE2013-11428: p. V006T11A022.

[14] Guarneri, A., Carminati, S., Zamora, M. and Roy, S., 2005. "Determining Mud Rheology For Optimum Hydraulics." In Offshore Mediterranean Conference and Exhibition, Ravenna, Italy, March 16-18, 2005. OMC-2005-018.